A Portable Self-Powered Turbine Spirometer for Rehabilitation Monitoring on COVID-19

Minghao Liu, Puchuan Tan, Jiangtao Xue, Zhuo Liu, Han Ouyang, Dongjie Jiang, Yuan Xi, Wei Sun, Yiqian Wang, Yansong Gai, Bojing Shi, Yang Zou, and Zhou Li**

Coronavirus disease 2019 (COVID-19) patients may experience persistent impairment of the lungs after recovery and discharge, which can cause a decline in pulmonary function. Therefore, regular pulmonary function tests are essential for COVID-19 recovered patients, and portable, home-based pulmonary function test devices are of great significance during the pandemic. Herein, a portable self-powered turbine spirometer (PSTS) is designed for respiratory flow measurement and assessment of pulmonary function with high accuracy, humidity resistance, good durability, and low cost. The respiratory airflow can directly drive PSTS to produce a sinusoidal signal with a signal-to-noise of 40.64 dB. By utilizing the long short-term memory (LSTM) model, the flow is successfully predicted, and the "lag-before-start" and "spin-after-stop" defects of the turbine spirometer are eliminated effectively. For pulmonary function tests, the flow-volume loop curve can be obtained from PSTS, and pulmonary function parameters such as inspiratory capacity (IC), forced vital capacity (FVC) and forced expiratory volume in the first 1 s (FEV_1) can be calculated. The accuracy of IC is over 95%, and others can reach over 97%. A portable smart pulmonary function assessment system is further developed and used to test the pulmonary function of COVID-19 patients one month after symptom onset, demonstrating potential for assessing rehabilitation trends and long-term follow-up of COVID-19 recovered patients.

1. Introduction

On 11 March 2020, the World Health Organization (WHO) declared coronavirus disease 2019 (COVID-19) to be a pandemic caused by severe acute respiratory syndrome coronavirus 2 (SARS-CoV-2).[1] Recent evidence suggests that the lungs are the organ most affected by COVID-19[2] with different pathophysiological damages,[3] leading to anomalies of pulmonary function happened in COVID-19 patients.[4] Moreover, some studies have shown that patients might experience persistent impairment of pulmonary function lasting for months or even years after COVID-19 recovery and discharge,[5] which could cause a decline in pulmonary function and ventilatory defects, symptoms of exercise intolerance, physical functioning decreasing, affecting the quality of life.[3,6] So regular pulmonary function tests and the long-term follow-up of COVID-19 recovered patients are essential.[4,7]

M. Liu, Y. Wang, Z. Li
Center on Nanoenergy Research
School of Physical Science and Technology
Guangxi University
Nanning 530004, China
E-mail: zli@binn.cas.cn

M. Liu, P. Tan, J. Xue, D. Jiang, W. Sun, Y. Wang, Y. Gai, Z. Li
Beijing Institute of Nanoenergy and Nanosystems
Chinese Academy of Sciences
Beijing 101400, China

P. Tan, H. Ouyang, Z. Li
School of Nanoscience and Technology
University of Chinese Academy of Sciences
Beijing 100049, China

J. Xue, Y. Zou
School of Life Science
Institute of Engineering Medicine
Beijing Institute of Technology
Beijing 100081, China
E-mail: zouyang@binn.cas.cn

Z. Liu, Y. Xi, B. Shi
Key Laboratory of Biomechanics and Mechanobiology
Ministry of Education
Beijing Advanced Innovation Center for Biomedical Engineering
School of Biological Science and Medical Engineering
School of Engineering Medicine
Beihang University
Beijing 100191, China

The ORCID identification number(s) for the author(s) of this article can be found under https://doi.org/10.1002/admt.202300328

DOI: 10.1002/admt.202300328

Spirometry is a commonly method of pulmonary function tests (PFTs), by using a pneumotachograph or spirometer, the flow-volume loop curves[8] and some important pulmonary function parameters[9] can be acquired to analyze the pulmonary airway ventilation of subjects. However, conventional pneumotachograph is only used in the hospital, and public medical resources are incredibly scarce during the COVID-19 pandemic, which brings inconvenience to patients needing home quarantine or long-term follow-up. Besides, the equipment needs to detect a large number of patients every day, leading to a risk of cross-infection and high maintenance costs.[10] Flow-measurement spirometer is becoming more popular because of its portability, automation, easy testing and analysis.[11] There are some portable home spirometers commercially available, however, either the function is too singular or the price is still high and not applicable to COVID-19 patients. Among the existing flow-measurement spirometers, the turbine spirometer is considered that the highest long-term stability.[12] Because it does not need frequent humidity, temperature, or air pressure correction, and it is not affected by altitude and gas composition.[11,13] The airflow volume that passes through turbine spirometers can be measured by mathematical models,[14] but they are unable to record the real time airflow speed accurately in PFTs. In addition, the signals generated from turbine always lag in actual airflow at the beginning of inspiration or expiration ("lag-before-start"), and at the end of inspiration or expiration, the turbine signals continue after the actual airflow has drop to 0 ("spin-after-stop"),[15] which may lead to a measurement error. Therefore, it is crucial to develop a portable, accurate, low-cost and durable device for assessing pulmonary function during the COVID-19 pandemic.

The Triboelectric nanogenerator (TENG) is an advanced energy harvesting or sensing technology in recent years, it is an expert in harvesting micromechanical energy to support other components or responding to micromechanical movements, such as airflow, pulse, and vibration, without any external power supply, thus generating signals.[16] As a self-powered sensor, TENG has attracted much attention due to its high sensitivity, fast response, and low cost. Some respiratory airflow sensors based on TENG have also been reported,[17] showing good response characteristics to airflow. However, the output performance of TENG sensor is likely affected by humidity and frictional loss.[18] Herein, we report a portable self-powered turbine spirometer (PSTS) based on floating rotary freestanding TENG (FRF-TENG) for respiratory flow measurement and assessment of pulmonary function. By the triboelectric effect and electrostatic induction, the turbine rotor converts low-frequency respiratory airflow to a full sinusoidal signal with a good signal-to-noise ratio (40.64 dB) when the airflow passes through. The PSTS shows high stability under different humidity and good durability after 500000 working cycles due to an airflow-electrode isolation design. The relationship between airflow speed and signal frequency of PSTS was established by theoretical derivation and experimental verification.

The long short-term memory (LSTM), a type of neural network, here is used to train and predict the flow. After training, the flow in every moment can be predicted according to the frequency feature, and the flow curve during the PFTs can be predicted successfully. Besides, the "lag-before-start" and "spin-after-stop" defects are eliminated simultaneously by LSTM. When performing one forced vital capacity through PSTS, the flow-volume loop curve can be obtained and pulmonary function parameters such as inspiratory capacity (IC), forced vital capacity (FVC), forced expiratory volume in the first 1 s (FEV_1), and FEV_1/FVC can be calculated. Integrating PSTS with a data acquisition and transmission module, a portable smart pulmonary function assessment system is also developed. The supporting software includes a desktop and mobile phone app that can display predicted flow and calculate pulmonary function parameters for further assessing pulmonary airway ventilation. The system was actually used to test pulmonary function in some volunteers infected with COVID-19, and three follow-up tests were performed within a month of symptom onset in one volunteer. The results obtained by PSTS compare favorably with commercial flowmeter with over 95% accuracy in IC, and over 97% accuracy in other pulmonary function parameters showing good potential for remote assessment of pulmonary rehabilitation trends and long-term follow-up of COVID-19 patients.

2. Results and Discussion

2.1. Overview and Structure Design of Portable Self-Powered Turbine Spirometer

As **Figure 1**a shows, the PSTS adopts a turbine structure and a floating rotary freestanding TENG (FRF-TENG), which consists of a stator (Figure 1a(i)), rotors (Figure 1a(ii)), base shell (Figure 1a(iii)) and some helper accessories. Optical photos of various parts and sizes of the TENG sensor are exhibited as Figure S1a (Supporting Information). The stator is composed of a PLA annular base and flexible electrodes with exposed copper, serving as the conductive layer of TENG. The rotating part has two rotors, the turbine rotor acts as a transducer, and the annular rotor acts as the dielectric layer of TENG. There are 12 units evenly and neatly arranged on the outer surface of the annular rotor, on which the polytetrafluoroethylene (PTFE) film and Nylon film alternately adhere. The two rotors are connected by a shaft, with both ends bearing a connection to reduce rotation resistance. The internal details and sectional view of TS are shown in Figure 1(a(I),a(II)). The annular rotor adopts a bent skeleton design that will not hinder airflow passage, allowing the rotor to rotate smoothly at the same time. Besides, the airflow-electrode isolation design is shown in Figure S2 (Supporting Information), its main function is to avoid moist respiratory airflow affecting the interaction of the dielectric layer with the conductive layer and improve humidity stability of the TENG sensor for flow measurement and PFTs. COVID-19 recovered patients always suffer from anomalies of pulmonary function, [3] because SARS-CoV-2 might persistently impair the lung and cause a decline in pulmonary function (Figure 1b). Figure 1c illustrates the process of PFTs using PSTS. When performing inspiration and one forced vital capacity, the low-frequency respiratory airflow drives the rotor to rotate continuously, generating a sinusoidal signal without an external power supply, then the flow is predicted through deep learning to assess the pulmonary function of subjects.

2.2. Working Principle and Output Performance of FRF-TENG

The illustration and working principle of the FRF-TENG (**Figure 2**a). A and B electrodes on the conductive layer are the

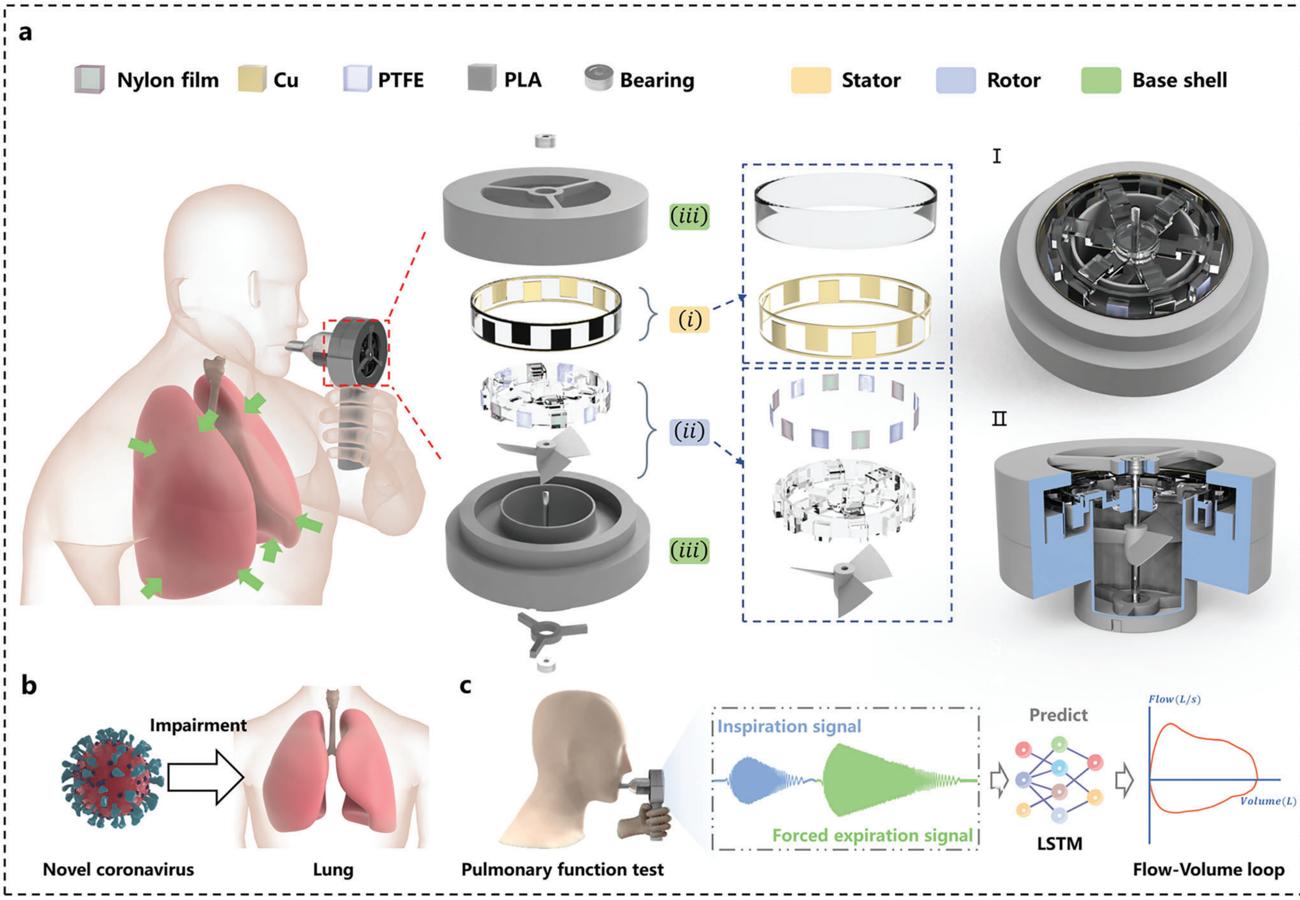

Figure 1. Overview of portable self-powered turbine spirometer (PSTS). a) Schematic diagram of the PSTS system and TENG sensor, internal details and sectional view of the TENG sensor, and materials used are shown. b) Schematic diagram of coronavirus impairs the lung. c) Prediction procedure from pulmonary function test signal to flow by LSTM neural network.

same size as the PTFE and Nylon films on the dielectric layer, and the spacing L1 between the electrodes is the same as the width L2 of the electrodes. The gap between the stator and the rotor is set to 1 mm to ensure no friction during rotation. There are four transient processes in one working cycle. In the initial state, the PTFE and Nylon films on the dielectric layer are facing the spacing between the electrodes on the conductive layer, and there is no potential between electrodes A and B because of no charge transfer. The potential reaches the maximum during the Figure 2a(i) process, because the PTFE with negative charges attracts positive charges in the copper electrodes to move, and the Nylon with positive charges also forces positive charges in the copper electrodes to move in the same direction, which leads the more charge transfer. As the interaction areas become larger, the transient transfer of charges becomes more and reaches the maximum. The potential drops during Figure 2a(ii) process because of the dielectric layer rotating forward, the interaction areas reducing causes a decreased ability to force charges to transfer. A reverse potential maximum occurs after Figure 2a(iii), when the dielectric layer and conductive layer face each other again, and finally return to the initial state by Figure 2a(iiii). A full sinusoidal signal is produced when a working cycle of FRF-TENG is completed. The conventional freestanding TENG(CF-TENG) working principle is as Figure 2b shows, only PTFE is used as the dielectric layer. In contrast, the FRF-TENG using PTFE and Nylon dielectric materials will generate more transferred charges, resulting in higher output (Figure 2c).

In order to verify the working principle of the FRF-TENG, a finite element analysis of the electric potential changes in dielectric and conductive layers during rotation is conducted by COMSOL Multiphysics (Figure 2d), which is consistent with the four processes previously analyzed. Besides, the electrical output performance of FRF-TENG with different combinations of dielectric materials is compared. The open-circuit voltage, short-circuit current, and charge transfer amount of the corresponding FRF-TENG are shown in Figure 2e,f,g, respectively. Obviously, the Nylon film helps significantly improve the output performance, and the thick PTFE also improves the output more effectively than the thin PTFE.

2.3. Theoretical Analysis and Characterization of PSTS

The turbine rotor drives the FRF-TENG to rotate when the airflow passes through it, converting the airflow to the sinusoidal signal. The sinusoidal signal frequency contains airflow characteristics,

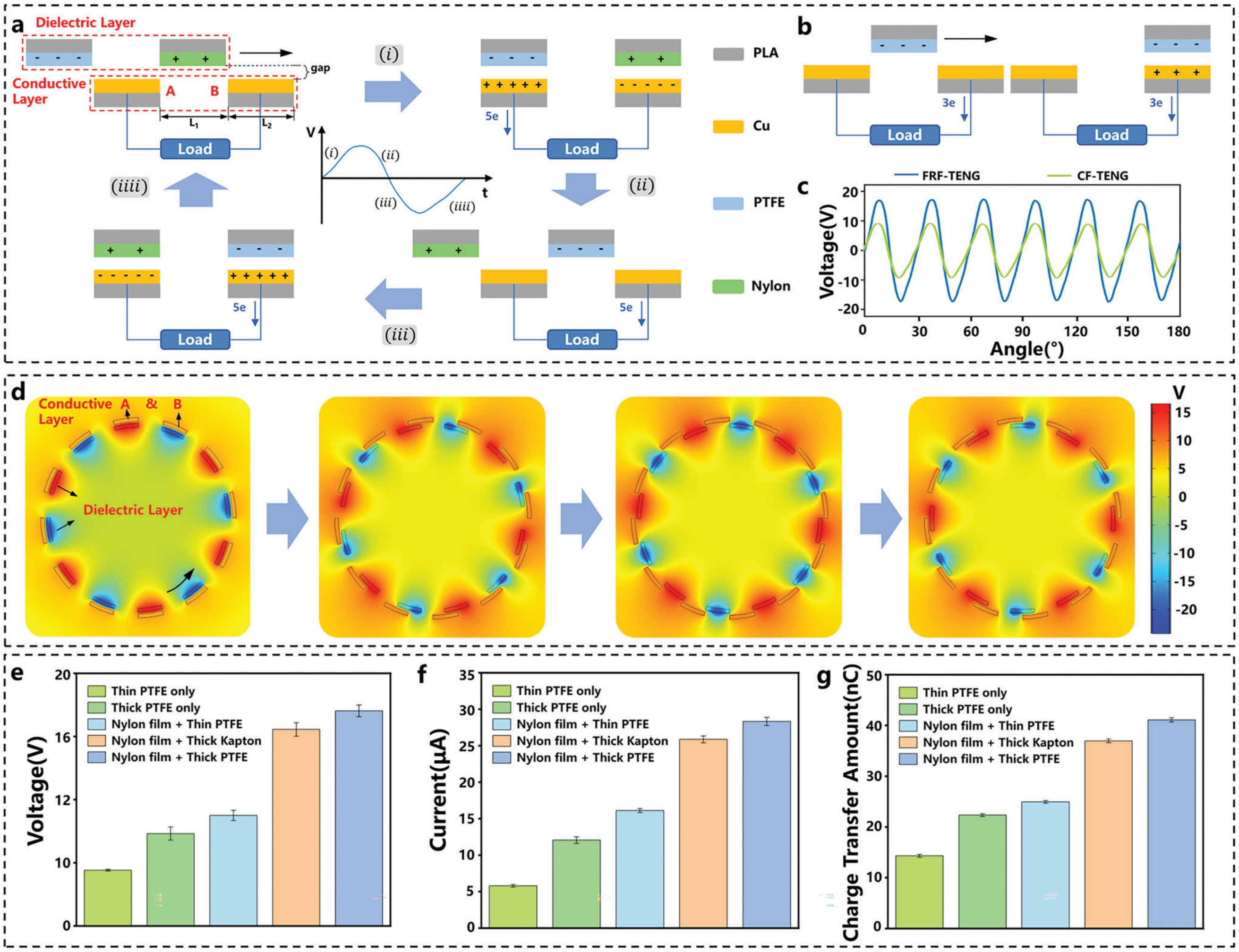

Figure 2. Working principle of FRF-TENG in rotation and different material output performance. a) Working principle of FRF-TENG and changes in charge transfer in the transient process. b) Working principle of the CF-TENG and changes in charge transfer in the transient process. c) The output performance comparison of FRF-TENG and CF-TENG. d) COMSOL simulation result of FRF-TENG in rotation. e–g) Output performance in different situations after one forced vital capacity.

which is a critical feature linking with the flow. Theoretically, the phenomenon of airflow drives the turbine rotor to rotate can be considered to explain by the air resistance model:

$$F = \frac{1}{2}\rho \cdot Cd \cdot S \cdot v^2 \tag{1}$$

The F is air drag, ρ is the air density, Cd is the drag coefficient, S is the area perpendicular to the airflow direction, v is the airflow speed. A test platform is built (**Figure 3**a), an air blower provides airflow at different speeds, an anemometer measures the airflow speed, and an oscilloscope is used to acquire the output signals and calculate signal frequency. As Figure 3b shows, when the airflow drives a single fan vane of the turbine rotor and the fan vane is going to rotate upwards, assume that the inclination angle of the fan vane to the vertical direction is θ, the total force acting on the fan vane will be resolved into an upward lift and a backward pressure. At the same time, there is an air drag that is horizontally opposite to the direction of rotation (Figure 3c).

Under the continuous action of the air blower, the rotors can rotate at a constant speed, which means that the lift is equal to the force that hinders the movement. The hindrance force includes air drag, bearing friction, and electrostatic force coming from the FRF-TENG. Therefore, according to the formula of total torque provides the angular acceleration, the angular acceleration of rotors can be expressed as:

$$a = \frac{M_{rotor} - M_b - M_{ef}}{I} \tag{2}$$

a is the angular acceleration of rotors, I is the total moment of inertia rotors and shaft. M_{rotor}, M_b, M_{ef} is the torque comes from the combined force on the rotors, friction between bearings and shaft, and electrostatic force, respectively, which can be described by the formula:

$$M_{rotor} = 3\iint \left(r \cdot \sigma_{rotor}\right) dS \tag{3}$$

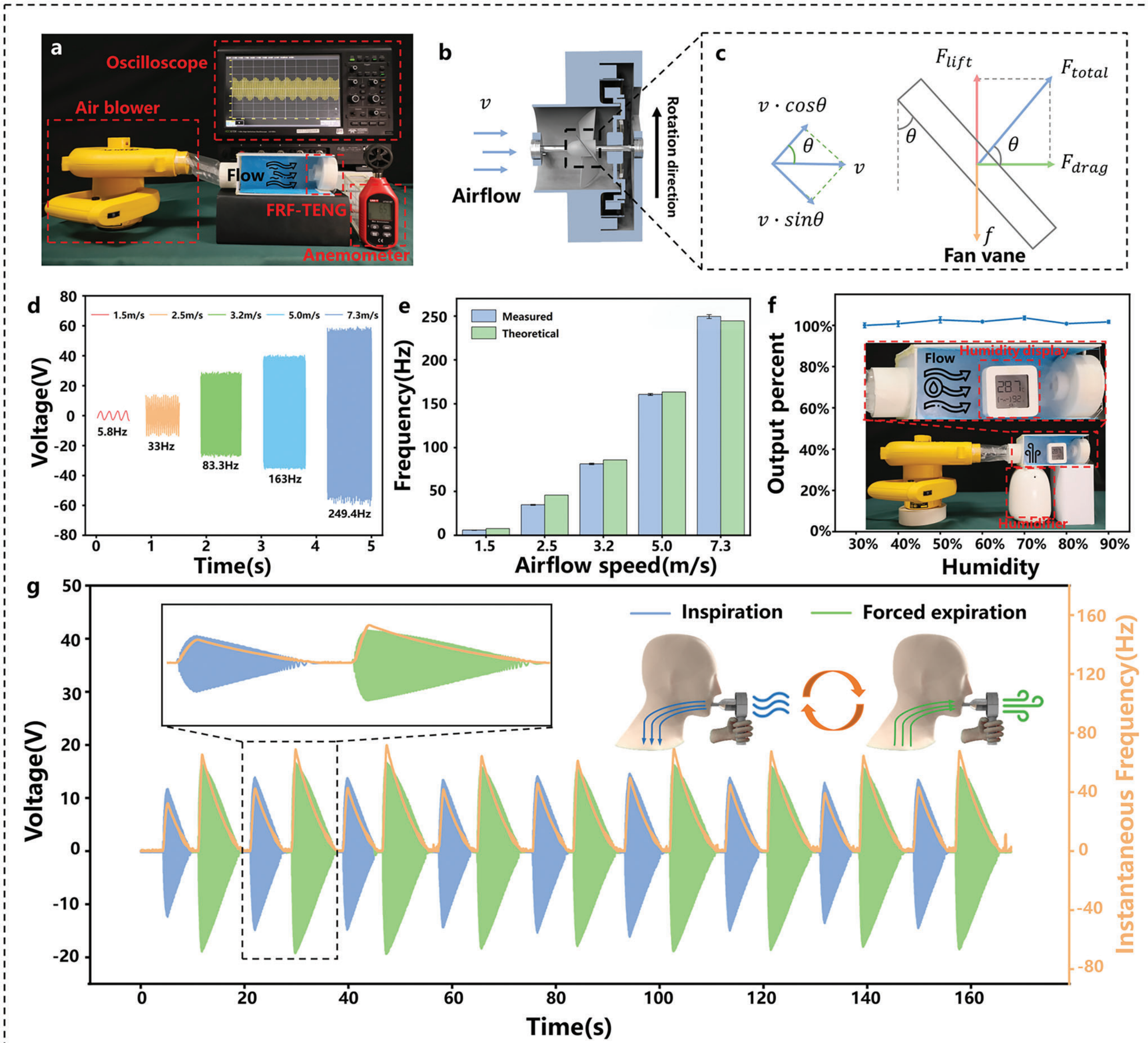

Figure 3. Theoretical model analysis and humidity stability of FRF-TENG sensor. a) Schematic diagram of the test platform. b) The sectional view of the FRF-TENG sensor. c) Force diagram of single fan vane when constant speed airflow passes through the fan vane. d) Output performances and measured frequency in different airflow speeds. e) Comparison of the measured frequency and theoretical frequency. f) Output performance under different humidity after one forced vital capacity. g) Continuous pulmonary function test signal and instantaneous frequency calculated from the signal.

$$M_b = 0.5 \cdot d \cdot \mu \cdot Pr \tag{4}$$

$$M_{ef} = 12 \iint \left(r \cdot \sigma_{ef}\right) dS \tag{5}$$

The σ_{rotor} is combined force per unit area of the fan vane, r is the radius distance to the σ_{rotor}, 3 means that there are three fan vanes on the turbine rotor. The d, μ, and Pr are bearing bore diameter, friction coefficient, and radial load, respectively. The σ_{ef} is the electrostatic force per unit area of a single parallel-plate capacitor, and there are 12 parallel-plate capacitors on the annular rotor. The σ_{rotor} and σ_{ef} can be expressed as:

$$\sigma_{rotor} = \frac{F_{lift}}{S_{vane}} - \sigma_{drag} \tag{6}$$

$$\sigma_{\mathrm{ef}} = \frac{F_{ef}}{S_{\mathrm{ppc}}} \tag{7}$$

S_{ppc} is the total area of parallel-plate capacitors. According to equation 1 and the electrostatic force formula:

$$F_L = \frac{1}{2}\frac{\varepsilon L}{g}V^2 \tag{8}$$

The F_{lift}, σ_{drag}, and F_{ef} can be expressed as:

$$F_{lift} = \frac{1}{2}\rho \cdot Cd \cdot S_{vane} \cdot v_{flow}^2 \cdot cos^2\theta \cdot sin\theta \tag{9}$$

$$\sigma_{drag} = \frac{1}{2}\rho \cdot Cd \cdot S_{vane} \cdot \omega_{rotor}^2 \cdot r^2 \cdot sin^3\theta \tag{10}$$

$$F_{ef} = \frac{1}{2}\frac{\varepsilon L}{g}V^2 \tag{11}$$

F_{lift} is the lift acted on the single fan vane, S_{vane} is the area of the single fan vane, σ_{drag} is the air drag per unit area of the single fan vane, ω_{rotor} is the angular velocity of the rotor when rotating, r is the radius distance to the unit area, L is the length of each side of a single capacitor, F_{ef} is the electrostatic force, which is related to the permittivity of free space ϵ, voltage V and gap g. To sum up, the angular velocity ω_{rotor} can be expressed (substitute the conditional parameters and calculate by Maple):

$$\frac{\partial}{\partial t}\omega + 0.02315890099\omega^2 - 29.33940278v^2 + 72.63904571 = 0 \tag{12}$$

ω_{rotor} would be calculated if the airflow speed v is given. There is a conversion between the frequency of the measured signal f_{signal} and angular velocity ω_{rotor}:

$$f_{signal} = \frac{3 \cdot \omega_{rotor}}{\pi} \tag{13}$$

The output voltage of the TENG sensor at different constant airflow speeds is acquired, which is able to detect the airflow as low as 1.5 m s^{-1}, and the corresponding signal frequencies are also measured (Figure 3d). The signal frequency shows an upward trend as the airflow speed increases. Furthermore, through theoretical calculation, the theoretical frequency under different airflow speeds is consistent with the measured frequency (Figure 3e). Therefore, the theoretical relationship between airflow and signal frequency from the TENG sensor is established successfully. Else, the output performance and frequency of the TENG sensor under higher airflow speed environments is shown in Figure S3 (Supporting Information). The voltage reaches a maximum of ≈70 V, while the frequency still increases by following the airflow speed increase. The upper limit of the response frequency may be higher, but because of the limited conditions of the laboratory, we can not get the maximum. Fortunately, the frequency range already met the application requirements. The detailed analysis process of airflow resistance on PSTS in working can be known in Note S1 (Supporting Information).

2.4. The Stability and Durability of PSTS

The expiration airflow of the human body is with high humidity (70%–90%).[19] In order to verify the humidity stability of the TENG sensor, an air humidifier and air blowers are used to simulate expiration airflow under varying humidity. Meanwhile, a hygrometer is used for real-time humidity detection. Figure 3f shows that the TENG sensor maintained a stable output under various humidity airflow, owing to the airflow-electrode isolation design to separate the electrodes and the airflow. While without the airflow-electrode isolation design, the output drops when humidity increase (Figure S4, Supporting Information). Therefore, the airflow-electrode isolation design can effectively prevent moist respiratory airflow from spreading to the electrode, and improve the humidity stability of the TENG sensor. Another experiment tests continuous output under changing humidity environment for ≈1 min, the result is shown in Figure S5a,b (Supporting Information). The voltage is maintained at 10 V when the airflow speed is 2.5 m s^{-1}, the corresponding frequency of the signal is ≈36 Hz. Both humidity tests evidence the humidity stability of the TENG sensor.

Considering temperature might affect the output performance of the TENG sensor, the validation of temperature stability is needed. The temperature experiment tests the output and signal frequency of the TENG sensor under varying temperatures after one forced expiration. The related curve is given in Figure S5c (Supporting Information), demonstrating the TENG sensor's stability in different temperature environments. Even though in a cold environment, the airflow-electrode isolation design can cope with moisture due to expiratory airflow condenses.

In addition, the durable properties of the TENG sensor are also tested by using an adjustable speed motor test system (Figure S5d, Supporting Information), the motor used is 620 rpm (Figure S5e, Supporting Information). The output signal can maintain high recognizability after 500000 working cycles (Figure S5f, Supporting Information). The reproducibility of PSTS is verified by the subject's PFTs, both voltage and instantaneous frequency keep stable after a couple of cycles of inspiration and forced expiration (Figure 3g), and the signal-to-noise ratio can reach 40.64 dB. Besides, by experimental test, The respiratory airflow speed can reach a maximum of 9–10 m s^{-1} through the disposable mouthpiece, and the instantaneous frequency is not more than 100 Hz.

2.5. The Process and Results of Deep Learning

The signal frequency of the TENG sensor constantly changes when performing PFTs, it is complicated to calculate flow from changing frequency. Long short-term memory (LSTM) is widely used for time series processing and predicting, the prediction is a process of calculating the target from features with the LSTM model. Here LSTM is used to predict flow from the instantaneous frequency of the signal. In this work, the target is flow acquired from a commercial flowmeter for flow calibration of PSTS in training and the features are instantaneous frequencies. **Figure 4**a shows the overview of the training process: smoothing, Butterworth lowpass filter, Hilbert transform, calculating instantaneous frequencies, downsampling, standardizing data scale, and converting to tensor are used in preprocessing before starting training. The sliding window divides the data into several sequences, which is conducive to predicting the target. In the training loop, the LSTM model predicts flow, and the optimizer helps

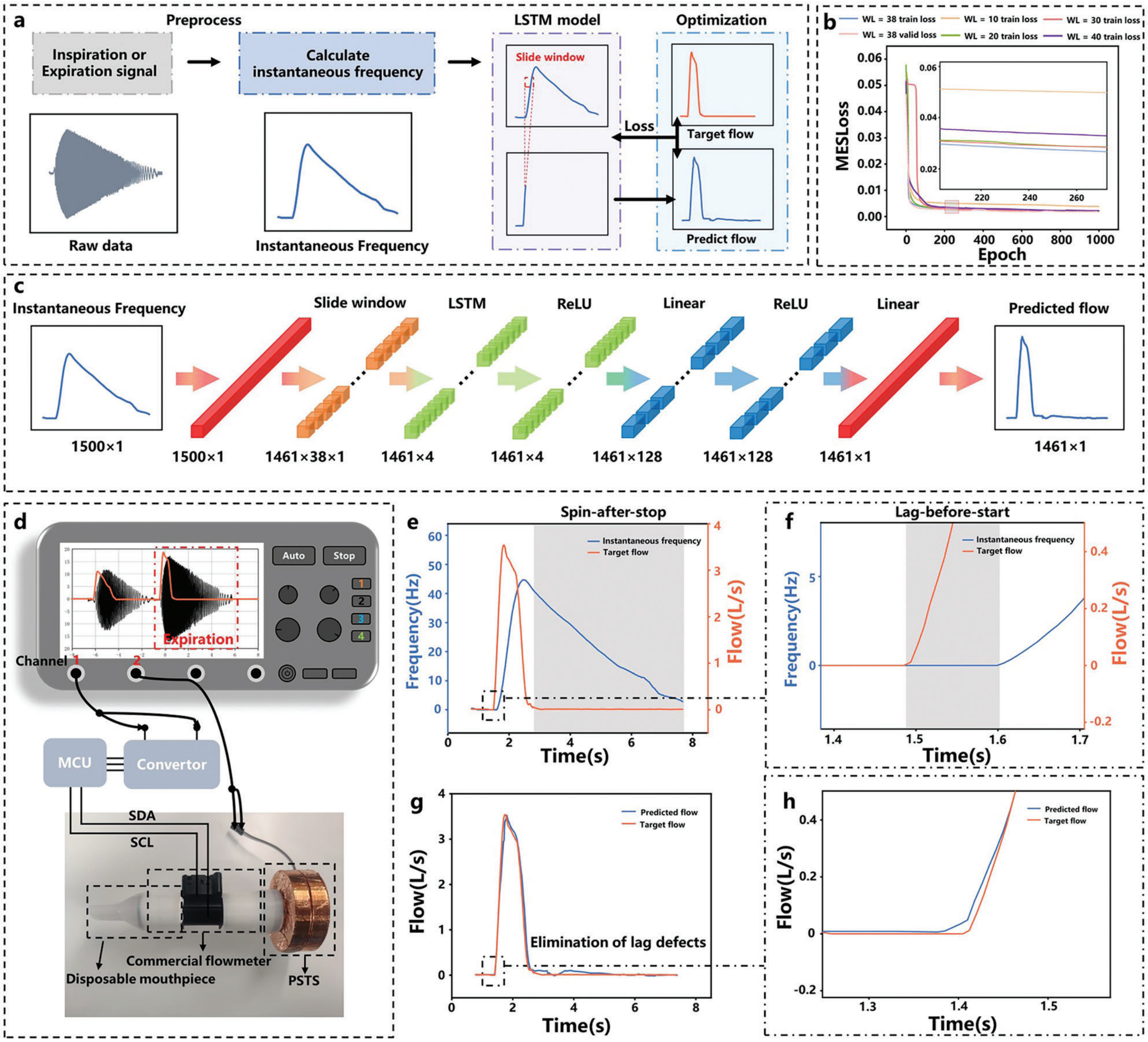

Figure 4. Processing methods and results of deep learning. a) Schematic diagram of deep learning. b) MSELoss in different window lengths (WL). c) Neural network structure based on LSTM. d) Schematic diagram of PSTS system calibration. The “spin-after-stop” e) and “lag-before-start” f) phenomena of expiration signal in PSTS compared with the target flow. g,h) Elimination of “lag-before-start” and “spin-after-stop” after prediction.

to optimize the model according to the loss. After training for 1000 epochs, there is a much lower loss, the lower means that the prediction is more consistent with the target. Different window lengths (WL) are varied, WL = 38 is the best WL parameter. The convergence of the mean-squared error loss (MSEloss) curve in different WL is shown in Figure 4b. The structure of the LSTM model includes 1 LSTpreM layer, 2 connected layers, and 2 activation layers (Figure 4c).

A PFTs platform based on PSTS is shown in Figure 4d, which is used to acquire samples for deep learning. The subject performed PFTs while the tightness of the system is ensured. The target flow used in training is provided by a commercial flowmeter. The raw signal and target flow on the oscilloscope screen come from one inspiration and forced expiration (Figure 4d). After preprocessing the raw signal to an instantaneous frequency curve, the lag defects: “lag-before-start” (≈100 ms) and “spin-after-stop” (a few seconds) of PSTS during forced expiration are found (Figure 4e,f). By the prediction of the LSTM model, the lag defects are eliminated effectively, and the predicted flow fits well with the target flow (Figure 4g,h). The “lag-before-start” and “spin-after-stop” of PSTS during inspiration and the predicted flow are exhibited in Figure S6a–e (Supporting Information)

The PSTS generates sinusoidal signals because the transfer of electrons is continuous during the rotor rotation and leads to continuous signals in the FRF-TENG. In comparison, the commercial turbine spirometer is based on a photoelectric sensor, which encodes the rotation of the turbine rotor into the square signals. The square signal acquired by the photoelectric sensor after one forced vital capacity is shown as Figure S7a (Supporting Information). By the same preprocessing method, the square signal's instantaneous frequency is extracted. And we found that sinusoidal signals are able to be extracted a complete instantaneous frequency curve, compared with the square signals by using the Hilbert transform (Figure S7a,b, Supporting Information). It means the sinusoidal signals include more frequency features that can be extracted to analyze. Therefore, the flow can be accurately predicted by the instantaneous frequencies from the sinusoidal signals. Furthermore, using the frequency feature can exclude the output voltage instability related to the surrounding environment, which improves the environmental stability of PSTS.

The PSTS will generate higher-frequency sinusoidal signals if more parallel-plate capacitor units are arranged. The higher-frequency sinusoidal signal is still with the same trend compared with lower-frequency sinusoidal signals, and there is a certain proportional relationship between them. Different from conventional turbine spirometers, the PSTS uses the LSTM model to predict the flow curve by the trend of signals, that is the instantaneous frequency (feature), and the normalization in preprocess eliminates the proportional relationship.

2.6. Portable Smart Pulmonary Function Assessment System

The respiratory flow is an essential target of PFTs. **Figure 5**a shows the changes in lung volume and shape when the subject performs PFTs, the lung contracts during expiration and relaxes during inspiration. The test method is inhaling to the maximum and then exhaling as quickly as possible to detect ventilatory defects. The ventilatory defect means the lung's elasticity and ability to open have been impaired, which will be reflected in the flow during PFTs. The ventilatory defect is a common abnormality of pulmonary function in COVID-19 recovered patients,[3,4] which can be classified as obstructive and restrictive. The obstructive ventilatory defect presents as $FEV_1/FVC<70\%$, while the restrictive ventilatory means lung volume decline, leading to a decrease of IC, FVC and FEV_1. To verify the availability of PSTS to COVID-19 patients, the PSTS was used to test and assess the pulmonary function of some volunteers infected with COVID-19. The flow-volume loop curve and PFT results of the volunteer (subject_0) before COVID-19 infection and 30 days after symptoms onset are shown in Figure 5b,c, respectively. Various degrees of decline in FEV_1, FEV_1/FVC and PEF are observed, indicating that the pulmonary function decline is still present for 30 days after symptoms onset. The PFT results of other subjects are shown in Table S1 (Supporting Information), the pulmonary function changes are not the same across subjects. Besides, three follow-up tests were also performed within 30 days of symptom onset in one volunteer (subject_3), the staged pulmonary function was recorded as shown in Table S2 (Supporting Information). The pulmonary function drops significantly in 10 days after symptoms onset and then recovers gradually, but the persistent impairment of pulmonary function still needs attention. From the above results, the pulmonary function of the subject can be assessed through PSTS with high accuracy (commercial flowmeter is used as a criterion): more than 95.08% in IC prediction, 97.47% in FVC prediction, 97.02% in FEV_1 prediction, 97.89% in FEV_1/FVC prediction and 98.70% in peak expiratory flow (PEF) prediction. Besides, the used model exhibits good linearity by correlation analysis between prediction and target shown in Figure S8a,b,c (Supporting Information), indicating the feasibility of combining PSTS and deep learning, leading to stronger prediction and generalization capabilities.

A portable smart pulmonary function assessment system is developed for real-time acquisition and analysis of respiratory airflow. The system composition block diagram is shown in Figure 5d, which includes four components: PSTS, signal processing module, power management module, and desktop app, and the optical photo of the system is shown in Figure 5e. The portable smart pulmonary function assessment system can acquire real-time signals, then some significant parameters associated with pulmonary function are analyzed to assess airway ventilation and displayed on the desktop app (Figure 5f). In order to highlight the portability of this system, we have also developed a mobile app. The signal can be transmitted to the mobile phone through the Bluetooth module, and the pulmonary function assessment can be realized on the mobile phone app (Figure 5g). Meanwhile, the pulmonary function assessment system also evaluates the severity of the ventilatory defect, which is of great significance to the diagnosis of chronic obstructive pulmonary disease (COPD) and pneumonia. The Video S1 (Supporting Information) depicts the real-time signal acquisition, flow prediction, and further analysis during the PFTs.

The portable smart pulmonary function assessment system is expected to be applied in functioning rehabilitation after COVID-19 recovery by following precise guidance according to follow-up of pulmonary function (Figure 5h). With recovery from COVID-19 often accompanied by a decline in physical functioning, remote PFTs can help document trends in airway ventilation and prevent more severe ventilatory defects and pneumonia. The recorded pulmonary function data can be further evaluated by experts and guided COVID-19 recovered patients by specific rehabilitation exercises to restore physical functioning

3. Conclusion

In summary, based on turbine structure and floating rotary freestanding triboelectric nanogenerator, a portable self-powered turbine spirometer (PSTS) is designed for flow measurement and assessment of pulmonary function, which can be driven to rotate by airflow speed as low as $1.5\mathrm{m\ s^{-1}}$ and generate sinusoidal signals. The signal-to-noise can reach 40.64 dB. The PSTS also shows high humidity resistance in different humidity environments, great stability and durability after 500000 working cycles. The relationship between signal frequency from PSTS and airflow speed is found by theoretical derivation and verified by experiment. With the help of LSTM model, PSTS can achieve accurate flow prediction and effectively eliminate the lag defect presented in turbine spirometers. Moreover, a portable smart pulmonary function assessment system based on PSTS is constructed to simplify pulmonary function testing and miniaturize test device. Some critical pulmonary function parameters such as IC, FVC, FEV_1, and PEF are able to be calculated accurately to assess airway ventilation. The accuracy reaches more than 95.08% in IC prediction, 97.47% in FVC prediction, 97.65% in FEV_1 prediction, 97.02% in FEV_1/FVC prediction, and 98.70% in PEF prediction. The developed system was further validated in testing and assessing

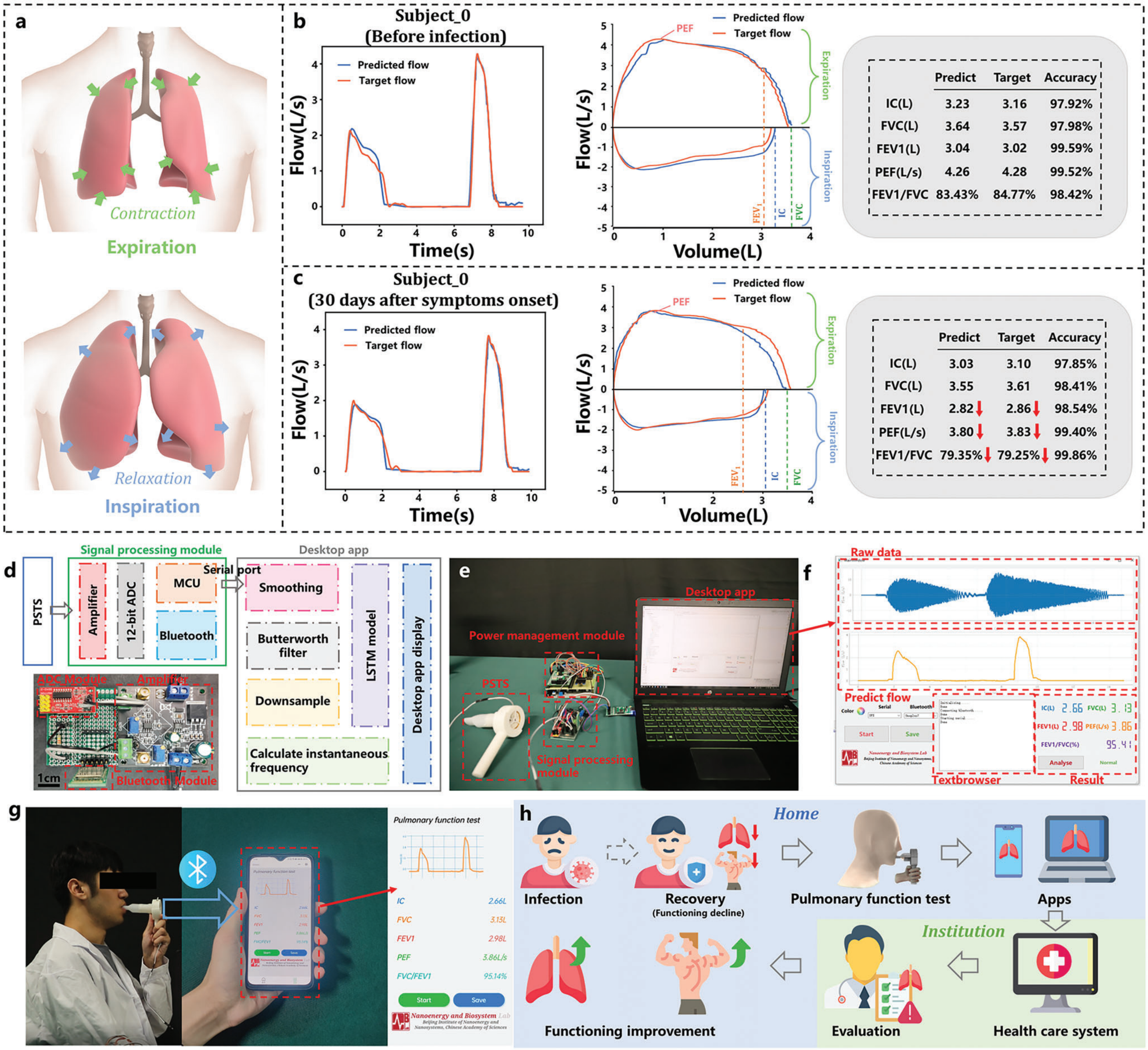

Figure 5. Portable smart pulmonary function assessment system based on PSTS. a) Schematic diagram of changes in lung morphology during respiration. b) Pulmonary function test result of subject_0 before COVID-19 infection. c) Pulmonary function test result of subject_0 30 days after symptoms onset. d) Schematic diagram of portable smart pulmonary function assessment system and optical photo of the signal processing module. e) Optical photo of portable smart pulmonary function assessment system. f) Desktop app interface of pulmonary function test. g) Exhibition of pulmonary function test result on the mobile phone app. h) Schematic diagram of functioning rehabilitation by following guidance according to follow-up of pulmonary function.

the pulmonary function of COVID-19 patients, showing the potential to remote PFTs, assess rehabilitation trends, and long-term follow-up of COVID-19 recovered patients.

4. Experimental Section

Design of PSTS Structure: The PSTS structure was designed by Solidworks2021, and prepared by 3D printing polylactic acid (PLA, RAISE3D E2 Technologies). The inner diameter of the annular structure as the electrode substrate was 40.8 mm, and the outer diameter was 44 mm (Figure S1a(I), Supporting Information), it can be fastened to the base (Figure S1a(VI), Supporting Information), there was a notch for wiring the electrodes out to read. The rotors shown in Figure S1a(II,IV) (Supporting Information) both were a lightweight design, 12 units evenly and neatly arranged on the outer surface of the annular rotor were for TENG fabrication. The base shell was made into a detachable mechanism, diameter and height were 56.79 and 22.36 mm, respectively, as shown in Figure S1c (Supporting Information) and S1d (Supporting Information). The protruding pipe was for disposable mouthpiece connections, and several millimeters of upper pipe extension, an airflow-electrode isolation structure, for isolating the expiration airflow from the electrode (Figure S1a(VI), Supporting Information).

Fabrication of the FRF-TENG Sensor: The PTFE with a thickness of 0.6 mm and Nylon film material was selected as the dielectric layer and pasted next to each other on the 12 units of the annular rotor after precisely cutting them into 5 mm × 5 mm size by using the laser cutting machine (VOIERN, WER1080 100 W). The copper electrode was selected as the conductive layer, the length, width, and thickness of the flexible electrode were 133, 7.4, and 0.14 mm, respectively. The copper, whose thickness was 35 µm, was exposed to air and made by immersion gold technology. The flexible electrode was pasted on the inner surface of the annular base by using Kapton tap.

Characterization and Measurements: An oscilloscope (LeCroy, HDO6104) was used for measuring the open-circuit voltage of the FRF-TENG sensor and storing the data. An electrometer (Keithley 6517) was used to measure the current and charge of the FRF-TENG sensor. Airflow was generated from an air blower (Stanley STPT600) with airflow speed control, A fan vane anemometer (UNI-T, UT363BT) was adopted to monitor the airflow speed in real-time.

Experimental Setup for Pulmonary Function Tests: A commercial flowmeter (Sensirion Flow Meters SFM3003) was employed to monitor real-time digital flow. Volunteers used a disposable mouthpiece and made sure respiratory airflow passes through the FRF-TENG sensor and commercial flowmeter simultaneously, record output curves on an oscilloscope (LeCroy, HDO6104) as samples. The abnormal pulmonary function data was from COVID-19 patients who were all symptomatic and confirmed positive by kit test. The participated volunteers were also co-authors of this manuscript. All participants had confirmed the details of the experiment and the signed informed consent was obtained from all participants prior to the research.

The Methods of Cleaning and Disinfecting the PSTS: After the pulmonary function test, the disposable mouthpiece should be thrown away, then the shell of PSTS was wiped by using 75% alcohol, and the inside of the tube was sprayed with 75% alcohol to disinfect at the same time. The alcohol does not affect the electrode due to the airflow-electrode isolation design. 75% alcohol was only preliminary disinfection. So UV lamps were used in fixed irradiation for 60 min, ensuring comprehensive disinfection.

Process of Deep Learning based on Pytorch (version 1.11): 1) Collect volunteers' pulmonary function test samples. 2) Divide the dataset (108 samples) into training set (88 samples), validation set (10 samples) and test set (10 samples) randomly. 3) Preparation of GPU (cuda version 11.3) for acceleration and important Pytorch libraries. 4) Data of training set need to be preprocessed: smoothing, filtering by Butterworth bandpass filter (<100 Hz), calculating instantaneous frequency by Hilbert Transform, downsampling to 1500 points, standardized the feature scale and target scale by calling StandardScaler method and MinMaxScaler method respectively which imported from sklearn libraries to avoid huge loss, convert to tensor through a sliding window which window length (WL) was 38. The shapes of data were formatted to [1461, 38, 1] tensors for input. 5) Define some important variables for training: number of epochs = 1000, learning rate = 0.0006, input size = 1 (number of features), hidden size = 4 (number of features in the hidden state), num layers = 1 (number of stacked LSTM layers), num classes = 1 (number of output classes), GPU acceleration during Training loop, calculate the loss by mean-squared error for regression (MSELoss), improve the weights by Adam optimizer step.

Supporting Hardware: MSP430-F149 (Texas Instruments) was developed for basic data processing and serial communication. The commercial flowmeter (Sensirion Flow Meters SFM3003, IIC communication protocol) was for flow calibration (provides target flow for calibration in deep learning training and comparison of accuracy in prediction), real-time digital flow was able to be read by MSP430-F149, linear transformation at the same time. Then the digital output was converted to an analog voltage signal by a frequency-voltage conversion chip (GP8101S) in order to record curve on the oscilloscope (LeCroy, HDO6104). The signal generated by FRF-TENG sensor was amplified through a commercial amplifier (DB207s). A 12-bit analog-to-digital converter (AD7705) was selected to collect the electrical signal in real time through the analog port. The Bluetooth module (HC-05) was connected to the "RXD" and "TXD" ports of the control chip MSP430-F149 (Texas Instruments).

Supporting Software: The supporting desktop software was developed based on Qt Designer (UI and interface) and Pycharm (functions), in order to acquire pulmonary function test signals to process, analyze, and display. The pulmonary function indicators (IC, FVC, FEV_1, PEF) were calculated (integral, comparison) from the predicted flow. The analysis methods refer to "Global Initiative for Chronic Obstructive Lung Disease" guidelines. And the mobile phone software was developed by WeChat Developer Tools based on JavaScript, it was able to read signals by Bluetooth technology.

The Methods of Pulmonary Function Assessment: The methods of pulmonary function assessment referred to global strategy for the diagnosis, management, and prevention of chronic obstructive pulmonary disease, 2022 report.[20]

Supporting Information

Supporting Information is available from the Wiley Online Library or from the author.

Acknowledgements

This study was supported by the National Natural Science Foundation of China (T2125003, 82202075), Beijing Natural Science Foundation (JQ20038), the Fundamental Research Funds for the Central Universities (E0EG6802X2), the National Postdoctoral Program for Innovative Talents (BX20220380), and China Postdoctoral Science Foundation (2022M710389). The authors thank everyone who contributed to this work.

Conflict of Interest

The authors declare no conflict of interest.

Data Availability Statement

The data that support the findings of this study are available from the corresponding author upon reasonable request.

Keywords

COVID-19, deep learning, pulmonary function tests, triboelectric nanogenerators, turbine spirometer

Received: March 1, 2023
Revised: April 9, 2023
Published online:

[1] C. Huang, Y. Wang, X. Li, L. Ren, J. Zhao, Y. Hu, L. Zhang, G. Fan, J. Xu, X. Gu, *Lancet* **2020**, *395*, 497.
[2] H. Shi, X. Han, N. Jiang, Y. Cao, O. Alwalid, J. Gu, Y. Fan, C. Zheng, *Lancet Infect. Dis.* **2020**, *20*, 425.
[3] X. Mo, W. Jian, Z. Su, M. Chen, H. Peng, P. Peng, C. Lei, R. Chen, N. Zhong, S. Li, *Eur Respir J* **2020**, *55*, 2001217.
[4] J. You, L. Zhang, J. Zhang, F. Hu, L. Chen, Y. Dong, K. Yang, B. Zhang, S. Zhang, *J Infect* **2020**, *81*, e150.
[5] a) D. Hui, G. Joynt, K. T. Wong, C. Gomersall, T. Li, G. Antonio, F. Ko, M. Chan, D. Chan, M. Tong, *Thorax* **2005**, *60*, 401; b) K.-C. Ong, A. W.-K. Ng, L. S.-U. Lee, G. Kaw, S.-K. Kwek, M. K.-S. Leow, A. Earnest, *Chest* **2005**, *128*, 1393.

[6] a) M. Thomas, O. J. Price, J. H. Hull, *Curr Opin Physiol* **2021**, *21*, 29; b) S. Talman, L. Boonman-de Winter, M. De Mol, E. Hoefman, R. Van Etten, I. De Backer, *Respiratory medicine* **2021**, *176*, 106272.
[7] a) R. Torres-Castro, L. Vasconcello-Castillo, X. Alsina-Restoy, L. Solís-Navarro, F. Burgos, H. Puppo, J. Vilaró, *Pulmonology* **2021**, *27*, 328; b) Y.-m. Zhao, Y.-m. Shang, W.-b. Song, Q.-q. Li, H. Xie, Q.-f. Xu, J.-l. Jia, L.-m. Li, H.-l. Mao, X.-m. Zhou, *EClinicalMedicine* **2020**, *25*, 100463.
[8] H. Bass, *Chest* **1973**, *63*, 171.
[9] J. L. Hankinson, B. Eschenbacher, M. Townsend, J. Stocks, P. H. Quanjer, *Eur Respir J* **2015**, *45*, 1283.
[10] a) J. Clausen, *Eur Respir J* **1997**, *10*, 1928; b) A. Kendrick, D. Johns, J. Leeming, *Respiratory medicine* **2003**, *97*, 1163; c) D. Hughes, D. Empey, *Br. Med. J.* **1972**, *4*, 470.
[11] D. J. F., *Breathe* **2008**, *4*, 251.
[12] A. Dirksen, F. Madsen, O. Pedersen, A. Vedel, A. Kok-Jensen, *Thorax* **1996**, *51*, 973.
[13] a) M. E. Aardal, L. L. Svendsen, S. Lehmann, T. M. Eagan, I. Haaland, *BMC Res. Notes* **2017**, *10*, 497; b) M. R. Miller, O. F. Pedersen, T. Sigsgaard, *J. Appl. Physiol.* **1997**, *82*, 1053; c) T. Adiono, N. Ahmadi, C. Saraswati, Y. Aditya, Y. P. Yudanto, A. Aziz, L. Wulandari, D. Maranatha, G. Khusnurrokhman, A. R. W. Riadi, R. W. Sudjud, *IEEE Trans Biomed Circuits Syst* **2022**, PP.
[14] a) Y. Sokol, R. Tomashevsky, K. Kolisnyk, presented at *2016 International Conference on Electronics and Information Technology (EIT)*, **2016**; b) M. Mhetre, Y. Patil, H. K. Abhyankar, *Innovations in Electronics and Communication Engineering* **2018**, https://doi.org/10.1007/978-981-10-3812-9_60587; c) L. Carretié, J. Iglesias, P. Aguilar, *Behavior Research Methods, Instruments, & Computers* **1997**, *29*, 582.
[15] M. P. Yeh, T. D. Adams, R. M. Gardner, F. G. Yanowitz, *J. Appl. Physiol.* **1987**, *63*, 1289.
[16] a) Y. Gai, E. Wang, M. Liu, L. Xie, Y. Bai, Y. Yang, J. Xue, X. Qu, Y. Xi, L. Li, D. Luo, Z. Li, *Small Methods* **2022**, *6*, 2200653; b) C. Li, D. Liu, C. Xu, Z. Wang, S. Shu, Z. Sun, W. Tang, Z. L. Wang, *Nat. Commun.* **2021**, *12*, 2950; c) J. Luo, Y. Li, M. He, Z. Wang, C. Li, D. Liu, J. An, W. Xie, Y. He, W. Xiao, Z. Li, Z. L. Wang, W. Tang, *Adv. Sci. (Weinh)* **2022**, *9*, 2105219; d) P. Tan, X. Han, Y. Zou, X. Qu, J. Xue, T. Li, Y. Wang, R. Luo, X. Cui, Y. Xi, L. Wu, B. Xue, D. Luo, Y. Fan, X. Chen, Z. Li, Z. L. Wang, *Adv. Mater.* **2022**, *34*, 2200793; e) Y. Cao, Y. Yang, X. Qu, B. Shi, L. Xu, J. Xue, C. Wang, Y. Bai, Y. Gai, D. Luo, Z. Li, *Small Methods* **2022**, *6*, 2101529.
[17] a) Q. Xu, Y. Fang, Q. Jing, N. Hu, K. Lin, Y. Pan, L. Xu, H. Gao, M. Yuan, L. Chu, Y. Ma, Y. Xie, J. Chen, L. Wang, *Biosens. Bioelectron.* **2021**, *187*, 113329; b) Y. Fang, J. Xu, X. Xiao, Y. Zou, X. Zhao, Y. Zhou, J. Chen, *Adv. Mater.* **2022**, *34*, 2200252; c) M. Wang, J. Zhang, Y. Tang, J. Li, B. Zhang, E. Liang, Y. Mao, X. Wang, *ACS Nano* **2018**, *12*, 6156.
[18] Q. Zheng, Y. Jin, Z. Liu, H. Ouyang, H. Li, B. Shi, W. Jiang, H. Zhang, Z. Li, Z. L. Wang, *ACS Appl. Mater. Interfaces* **2016**, *8*, 26697.
[19] E. Mansour, R. Vishinkin, S. Rihet, W. Saliba, F. Fish, P. Sarfati, H. Haick, *Sens. Actuators, B* **2020**, *304*, 127371.
[20] G. S. Committee, *GOLD Scientific Committee* **2022**.

